JM PAPERS

Computations of viscous fingering in a wedge: selection mechanisms and capillarity-driven ripples in the small surface tension limit

Cecilie Andersen[1] , **Philippe H. Trinh**[1] **and Jean-Marc Vanden-Broeck**[2]

[1]Department of Mathematical Sciences, University of Bath, Bath BA2 7AY, UK
[2]Department of Mathematics, University College London, London WC1E 6BT, UK
Corresponding authors: Cecilie Andersen, ca751@bath.ac.uk; Philippe H. Trinh, p.trinh@bath.ac.uk

We present a numerical scheme that solves for the self-similar viscous fingers that emerge from the Saffman–Taylor instability in a divergent wedge. This is based on the formulation by Ben Amar (1991, *Phys. Rev. A*, vol. 44, pp. 3673–3685). It is demonstrated that there exists a countably infinite set of selected solutions, each with an associated relative finger angle, and furthermore, solutions can be characterised by the number of ripples located at the tip of their finger profiles. Our numerical scheme allows us to observe these ripples and measure them, demonstrating that the amplitudes are exponentially small in terms of the surface tension; the selection mechanism is driven by these exponentially small contributions. A recently published paper derived the selection mechanism for this problem using exponential asymptotic analytical techniques, and obtained bifurcation diagrams that we compare with our numerical results.

1. Introduction

Saffman–Taylor viscous fingering is a classic problem in Hele-Shaw flows (Saffman & Taylor 1958): an inviscid (or less viscous) fluid is injected into a Hele-Shaw cell filled with a viscous fluid, and the interface between the fluids converges to a steady state with a single finger propagating along the length of the channel.

The proportion of the finger width to the channel width, λ, is a key parameter of the problem. It has been shown that a selection mechanism occurs in the small surface tension

limit $\epsilon \to 0$, where ϵ is the surface tension parameter (cf. Vanden-Broeck (2010) and references therein). A countable family of λ values is selected, which can be labelled $1/2 < \lambda_1(\epsilon) < \lambda_2(\epsilon) < \cdots < \lambda_n(\epsilon) < \cdots < 1$. Identifying the selected λ values and the associated solutions has been the focus of a number of works. A numerical scheme developed by McLean & Saffman (1981) and Vanden-Broeck (1983) was used to plot the bifurcation diagram. Analytical works have relied on the developing methods in beyond-all-order asymptotics to derive the selection mechanism (Hong & Langer 1986; Combescot *et al.* 1986, 1988; Tanveer 1987, 2000; Chapman 1999).

This paper considers a similar, but more complex, selection mechanism observed in an associated problem with a Hele-Shaw cell in the shape of a wedge with angle θ_0. The classic channel problem described above is given by the limit where $\theta_0 = 0$. The Hele-Shaw cell is filled with a viscous fluid, and an inviscid fluid is injected from the corner of the wedge. The interface between the fluids again develops a finger shape, which propagates outwards away from the corner of the wedge (this is observed experimentally in Paterson 1981; Thomé *et al.* 1989). In the general circular Saffman–Taylor problem, fluid is injected outwards in all directions from a central source, and a number of fingers develop on the fluid interface. Each of these fingers occurs, approximately, in a wedge with angle $\theta_0 > 0$. The interface near the tip of one of these fingers (away from the far-field regime at the source) can be approximated using the Saffman–Taylor problem in a wedge geometry.

In the recent work by Andersen *et al.* (2024), the authors employed techniques in exponential asymptotics to derive the selection law for Saffman–Taylor fingering in the wedge. This work built on an existing set of extensive analytical and numerical works by Brener *et al.* (1990), Ben Amar (1991*a*,*b*), Tu (1991), Levine & Tu (1992) and Combescot (1992).

In this paper, we construct a numerical scheme that is capable of solving the Saffman–Taylor problem in a wedge with $\theta_0 > 0$. This is significantly more complicated than the channel problem ($\theta_0 = 0$) solved in McLean & Saffman (1981) and Vanden-Broeck (1983) due to the additional complexities of the governing equations. Our numerical scheme has improvements in speed compared with using standard Newton solvers, and is capable of resolving the solution to small values of the surface tension parameter. With this scheme, exponentially small ripples on the numerical solutions are characterised for the first time, and we are able to demonstrate agreement with the recent analytical results of Andersen *et al.* (2024). Comparison between numerical and exponential asymptotic results for the Saffman–Taylor problems has not been presented before.

2. Mathematical formulation

Consider a Hele-Shaw cell with very small thickness compared to the length. The cell has a wedge shape with internal angle θ_0, and is filled with viscous fluid. An inviscid fluid is injected from the corner of the wedge at a prescribed flow rate, and displaces the viscous fluid to form a petal/finger shape (figure 1a). Eventually, as is seen experimentally (Thomé *et al.* 1989), a self-similar shape is reached where a finger occupies an angle $\lambda\theta_0$, with $0 < \lambda < 1$. Ben Amar (1991*a*) refers to this set-up as 'divergent flow'.

On the free surface, we solve for $q\,e^{-i\tau}$ (these are analogues of the speed q and streamline angle τ, and reduce to the actual fluid speed and streamline angle in the limit $\theta_0 \to 0$) and finger shape $\hat{z} = \hat{x} + i\hat{y}$. We transform the self-similar physical plane $\hat{x} + i\hat{y}$ (figure 1) into an infinite strip in a channel using the conformal map

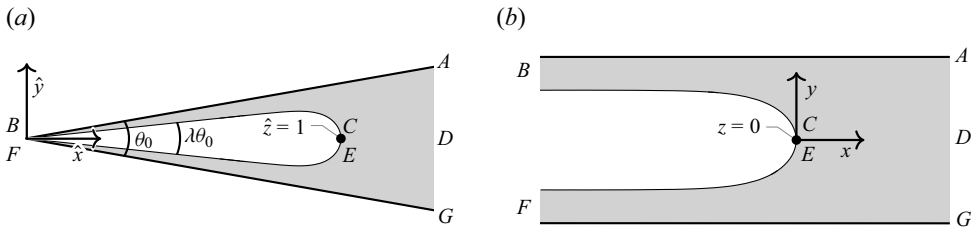$$z = \tfrac{2}{\theta_0} \log(\hat{z}). \tag{2.1}$$

Figure 1. (*a*) Top-down view of the numerically obtained physical profile in the $\hat{z}$-plane for the zero surface tension case with $\theta_0 = 20°$ and $\lambda = 0.6$. The Hele-Shaw cell is bounded by the thick black lines and is filled with a viscous fluid (grey). An inviscid fluid is injected from the corner of the wedge (BF at $\hat{z} = 0$) and forms a finger with angle $\lambda\theta_0$. The tip of the finger lies at $\hat{z} = 1$ (CE). (*b*) A numerical plot of the z-plane (obtained using the mapping (2.1)) is shown for the zero surface tension case with $\theta_0 = 20°$ and $\lambda = 0.6$. The tip of the finger lies at the origin (CE).

In figure 1(*b*), we show the image of the finger from figure 1(*a*) under this map. The walls BA and FG lie on $\mathrm{Im}(z) = \pm 1$, respectively, and the tip CE is fixed at the origin $z = 0$.

The independent variable is given as in Vanden-Broeck (1983), by $s = e^{-\pi f^*}$. Here, f^* is a generalised velocity potential as defined in Ben Amar (1991*a*, p. 43), and is chosen so that the streamline value $\mathrm{Im}(f^*)$ is constant on the free surface. Under this map, half the free surface (BC) lies on the real s-axis between 0 and 1, with the finger tip (C) at $s = 1$.

We require a set of governing equations for the unknowns $(x(s), y(s), q(s), \tau(s))$. Once these are solved for numerically, we can obtain a profile for the free surface in the physical wedge, $\hat{x} + i\hat{y}$, by reversing (2.1).

First, on the free surface, continuity of pressure yields Bernoulli's equation

$$\epsilon^2 \frac{\lambda}{Q_0} qs \frac{\partial}{\partial s}\left(r(x)\left[qs\frac{\partial\tau}{\partial s} + \frac{\ell}{2}\sin\tau\right]\right) - q = \frac{q}{1-\lambda} + \frac{q\lambda}{\pi Q_0}\int_0^1 \frac{K(t)}{t-s}\,\mathrm{d}t. \qquad (2.2)$$

In (2.2), we have defined the following functions for convenience:

$$r(x(s)) = \exp(-\theta_0\, x(s)/2) \quad \text{and} \quad K(s) = \frac{\sin[\tau(s)]}{q(s)\,[r(x(s))]^2}. \qquad (2.3)$$

In (2.2), we have also defined the dimensionless fluid flux constant Q_0, and the scaled interior wedge angle ℓ, to be

$$Q_0 = -\frac{1-\lambda}{\pi}\int_0^1 \frac{K(t)}{t}\,\mathrm{d}t \quad \text{and} \quad \ell = \ell(\lambda) = \frac{\theta_0}{\pi}(1-\lambda), \qquad (2.4)$$

where λ is the proportional finger angle parameter. Finally, we have introduced the key non-dimensional parameter ϵ by

$$\epsilon^2 = \frac{4\pi^2\sigma}{(1-\lambda)^2}, \qquad (2.5)$$

where σ is a modified surface tension parameter

$$\sigma = \frac{b^2}{12\mu}\frac{T}{R_0^3}\frac{1}{\theta_0^2} \qquad (2.6)$$

as in Ben Amar (1991*b*). Here, b is the distance between the plates in the Hele-Shaw cell, μ is viscosity, T is surface tension, and R_0 is a length scale parameter (the length from the wedge corner to the tip of the finger at time zero). Typically, we are interested in small surface tension, thus small values of ϵ.
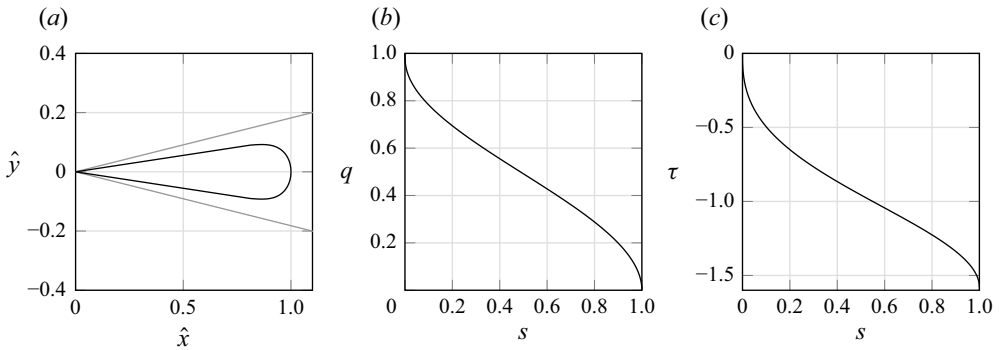
Figure 2. (*a*) Plot of a numerical solution shown in the $(\hat{x}, \hat{y})$-plane in the wedge. (*b,c*) Plots of the numerical solutions for the dependent variables $q(s)$, $\tau(s)$. In this figure, the parameter values are $\theta_0 = 20°$, $\epsilon^2 = 1$ and $\lambda = 0.64$.

Analyticity of $q\, e^{-i\tau}$ in the upper half s-plane gives, by the Hilbert transform,

$$\log q(s) = -\frac{s}{\pi} \int_0^1 \frac{\tau(t)}{t(t-s)}\, dt. \tag{2.7}$$

Finally, we close the system with

$$x(s) + i\, y(s) = -\frac{1-\lambda}{\pi} \int_s^1 \frac{e^{i\tau(t)}}{t\, q(t)}\, dt. \tag{2.8}$$

Thus the full system consists of equations (2.2), (2.7) and (2.8) for the unknowns (x, y, q, τ). The appropriate boundary conditions at $s = 0$ and $s = 1$ are

$$x(0) = -\infty, \quad y(0) = 1, \quad q(0) = 1, \quad \tau(0) = 0, \tag{2.9a}$$

$$x(1) = 0, \quad y(1) = 0, \quad q(1) = 0, \quad \tau(1) = -\frac{\pi}{2}. \tag{2.9b}$$

The governing equations can be compared with Ben Amar (1991*b*) equations (3.15)–(3.17). An example of the numerically obtained solutions for $\theta_0 = 20°$, $\epsilon^2 = 1$ and $\lambda = 0.64$ is shown in figure 2.

We note that following Ben Amar (1991*a*), the mathematical model of divergent flow developed here produces a steady-state formulation corresponding to an assumption of self-similarity of the original system. In particular, the spatial coordinates of the original system are assumed to scale with a time-dependent dimensionless scaling factor ((2.1) of Andersen *et al.* 2024).

3. Exponential asymptotics

We briefly present the exponential asymptotics method that can be used to derive the selection condition in the limit $\epsilon \to 0$. The full details of this are presented in Andersen *et al.* (2024), but we compare their results to our numerical results in § 6. The exponential asymptotic analysis involves approximating the dependent variables as asymptotic series in the small parameter ϵ,

$$x \sim \sum_{n=0}^{\infty} \epsilon^{2n} x_n, \quad y \sim \sum_{n=0}^{\infty} \epsilon^{2n} y_n, \quad q \sim \sum_{n=0}^{\infty} \epsilon^{2n} q_n, \quad \tau \sim \sum_{n=0}^{\infty} \epsilon^{2n} \tau_n. \tag{3.1}$$

The leading-order solutions $\{x_0, y_0, q_0, \tau_0\}$ are found analytically as shown in Andersen *et al.* (2024) equations (3.7) and (3.8). A plot of the leading-order physical profile (x_0, y_0) is shown later, in figure 5. The asymptotic series in (3.1) turn out to be divergent, and it is necessary to truncate them. If this is done at an optimal point $n = \mathcal{N}$, then the remainder will be a sum of contributions that are exponentially small in the surface tension parameter ϵ. For example, q will have the form

$$q \sim \sum_{n=0}^{\mathcal{N}} \epsilon^{2n} q_n + A_1 Q \, e^{-\chi_1/\epsilon} + A_2 Q \, e^{-\chi_2/\epsilon} + \cdots . \tag{3.2}$$

Exponential asymptotics techniques can be used to derive the forms of the components A_i, Q and χ_i as functions of s. These are given in terms of a different independent variable, ζ, in Andersen *et al.* (2024) (equations (6.16), (5.9) and (5.7)), where

$$s = \frac{1}{\zeta^2 + 1}. \tag{3.3}$$

The functions χ_i are complex functions and are given in terms of ζ by

$$\chi_i(\zeta) = -\int_{\zeta_i}^{\zeta} \frac{2\tilde{\zeta}\sqrt{\sin \tau_0 + \mathrm{i}\cos \tau_0}}{(1 + \tilde{\zeta}^2) q_0 \, r (x_0)^{3/2}} \, \mathrm{d}\tilde{\zeta}. \tag{3.4}$$

Here, ζ_i are locations of singularities in the complex ζ-plane (e.g. for $\theta_0 = 20°$, $\lambda = 0.75$, there is a singularity at $\zeta_1 = 0.62 + 3.01\mathrm{i}$). Since the χ_i are complex, the remainder terms introduce exponentially small oscillations in the solution with amplitudes $|A_i Q| \, e^{-\mathrm{Re}(\chi_i)/\epsilon}$. These oscillations can be seen on the tips of the fingers in figure 5. By enforcing the far-field boundary conditions (2.9*a*) on the remainder terms, it is possible to obtain the selection condition

$$\frac{|\Lambda_1|}{|\Lambda_C|} e^{-\mathrm{Re}(\chi_1(0))/\epsilon + \mathrm{Re}(\chi_C(0))/\epsilon} \cos\left(\arg(\Lambda_1) + \frac{\pi}{2} - \frac{\mathrm{Im}(\chi_1(0))}{\epsilon}\right)$$
$$+ \frac{1}{2} \cos\left(\arg(\Lambda_C) + \frac{\pi}{2}\right) = 0. \tag{3.5}$$

By symmetry arguments, only remainder terms related to two singularities (indexed '1' and 'C') contribute to the selection condition. The constants Λ_1 and Λ_C can be found with further analysis (see Appendix C of Andersen *et al.* 2024). Bifurcation diagrams can be plotted showing the solutions that satisfy (3.5), and these are presented in figure 8 in § 6 as a comparison to our numerical results.

4. Channel problem ($\theta_0 = 0$)

By taking the limit of the wedge angle, $\theta_0 \to 0$, we recover the classic Saffman–Taylor problem in a channel with parallel walls. This exhibits a similar selection mechanism for the relative finger widths, $0.5 < \lambda_1 < \lambda_2 < \lambda_3 < \cdots < 1$. The problem was solved numerically by McLean & Saffman (1981) and Vanden-Broeck (1983), who plotted bifurcation diagrams of the selected λ values against the surface tension parameter ϵ^2. We have replicated their numerical method to generate the bifurcation diagram in figure 3.

The analysis in § 3 can also be repeated for the simpler problem in a channel that is equivalent to taking the limit $\theta_0 \to 0$ in (3.5). The selection condition for the channel was first derived using exponential asymptotic techniques in Chapman (1999), and the selected λ values are presented in figure 3.
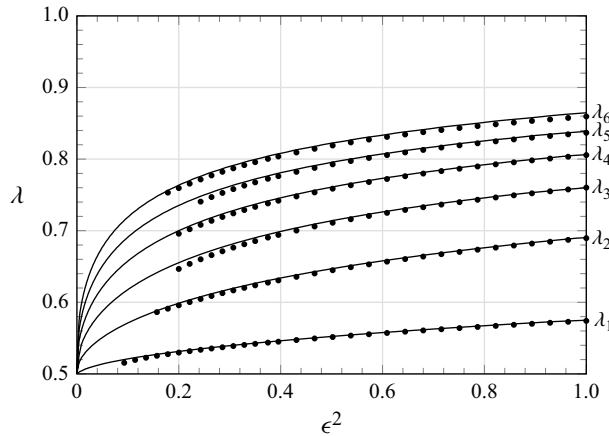
Figure 3. Bifurcation diagram for the Saffman–Taylor problem in a channel ($\theta_0 = 0$) showing the first six selected λ values for different values of the surface tension parameter ϵ^2. The black curves show the predicted branches from the exponential asymptotic analysis as done in Chapman (1999). The dots show the branches predicted using an implementation of the numerical scheme from McLean & Saffman (1981) and Vanden-Broeck (1983) with $N = 1000$ mesh points.

This comparison of numerical and exponential asymptotic results for the channel problem is currently missing from the literature. We see that the results agree well except for very small values of ϵ where larger numbers of mesh points in the numerical scheme would reduce the numerical errors. The Saffman–Taylor problem in a wedge poses additional difficulties in both the numerics and asymptotic analysis since the Bernoulli equation becomes more complex. In § 5, we describe a numerical method that can obtain numerical solutions of the wedge problem, and in § 6, we compare the bifurcation diagrams with recent exponential asymptotic results.

5. Numerical methodology

Our numerical method is a generalisation of methods from McLean & Saffman (1981) and Vanden-Broeck (1983), but with additional difficulties from the increased complexity of the equations. First, we relax the condition for the angle at the tip of the finger, $\tau(1)$, in (2.9b) so $\tau(1)$ becomes a free parameter to be solved for as part of the solution. We then solve for the physical profile at all combinations of ϵ^2 and λ. Each of these solutions will have an associated $\tau(1)$ value. Selecting the solutions with $\tau(1) = -\pi/2$ will give the physical fingers with a smooth tip. We now describe the scheme in more detail.

Following McLean & Saffman (1981) and Vanden-Broeck (1983), we introduce a stretched mesh from $s \mapsto \xi$ defined by

$$s^\rho = 1 - \xi^\gamma, \tag{5.1}$$

where ρ solves the equation

$$\frac{\cot(\pi\rho)}{\rho^2} = \frac{\epsilon^2 \theta_0^2}{4}. \tag{5.2}$$

The parameter γ defines the distribution of mesh points, with a larger γ meaning that more points are distributed near the tip of the finger. For the results in this paper, we choose $\gamma = 4$, as is done in Vanden-Broeck (1983). A larger value of γ means that more accurate

results can be achieved with fewer mesh points. If γ becomes too large (e.g. $\gamma \gtrsim 5$), then the numerical scheme fails to converge.

The principal mesh points and their related midpoints are respectively defined by $\xi_j = j/N$ for $j = 0, 1, \ldots, N$, and $\xi_j^m = (2j-1)/2N$ for $j = 1, 2, \ldots, N$, and the corresponding points in the s-plane are found using (5.1). The unknowns are the values of τ at the mesh points, which we denote $\tau_j = \tau(s_j)$ with $j = 0, 1, \ldots, N$. The condition $\tau(0) = 0$ from (2.9a) fixes $\tau_N = 0$. We allow $\tau_0 = \tau(1)$ to be a free parameter, so we have N unknowns, $\tau_0, \ldots, \tau_{N-1}$. We will similarly use subscripts when evaluating other variables at mesh points, i.e. $q_j = q(s_j)$, $x_j = x(s_j)$ and $y_j = y(s_j)$.

The main step in the numerical scheme is evaluating (2.2) at the $N-1$ internal mesh points, $s_1, \ldots, s_{N-1}$, to give $N-1$ equations:

$$\epsilon^2 s_j \left(r(x_j) \left[q_j s_j \tau_j' + \frac{\ell}{2} \sin \tau_j \right] \right)' + \frac{Q_0}{1 - \lambda} + \frac{1}{\pi} I(s) = 0, \quad j = 1, \ldots, N-1. \quad (5.3)$$

In (5.3), we have used the definitions of $r(x)$ from (2.3) and ℓ from (2.4). It is also convenient to define the integral

$$I(s) = \int_0^1 \frac{K_j(t)}{t - s} \, \mathrm{d}t, \quad (5.4)$$

where $K_j = K(s_j)$. We use trapezoidal rules to evaluate the integrals in (5.3) from x_j (2.8), q_j (2.7), Q_0 (2.4) and I.

We have defined $N-1$ equations in (5.3) for the N unknowns ($\tau_0, \ldots, \tau_{N-1}$). To close the system, we introduce one final equation, which is given by evaluating the trapezoidal approximation of (2.8) in the far-field, at $s = 0$,

$$\lambda - \mathrm{Im} \left[\frac{1 - \lambda}{\pi N} \sum_{k=1}^{N-1} \frac{\sin(\tau_k) s_k'}{s_k q_k} \right] = 0. \quad (5.5)$$

That is, (5.3) and (5.5) give N equations that can be solved for the N unknowns using a Newton iteration scheme.

In practice, the evaluation of the equations is computationally intense due to the number of integrals approximated with trapezoidal rules. The Jacobian matrix is dense, so the equations must be evaluated many times at each step.

In order to speed up the scheme, we use Broyden's method (Broyden 1965), which is a quasi-Newton method. Broyden's method evaluates the Jacobian only on the first step, then updates the associated matrix to approximate the Jacobian at later steps. However, the method requires a much closer initial guess than Newton's method to converge. We therefore implement a scheme that uses Newton's method at low N values (typically $N = 250$) to provide an interpolated approximation for the initial guess to the Broyden scheme at higher values of N (e.g. $N = 500$). We continue doubling N, interpolating the solution and solving with Broyden until we reach the desired value of N. Using this scheme, we can obtain a solution for $N = 2000$ almost five times faster than using pure Newton's method. The run times of this scheme compared to the standard Newton's method are shown in table 1. We find that the convergence rate of the numerical scheme is $\mathcal{O}(1/N)$ as $N \to \infty$, therefore a large value of N is needed to obtain accurate results.

θ_0	λ	ϵ^2	N	γ	Newton time	Broyden–Newton time	Ratio
20°	0.8	0.5	2000	4	950	210	4.5
20°	0.8	1	1000	4	160	54	3.0
20°	0.8	0.1	1000	4	130	50	2.6
20°	0.7	1	1000	2	130	52	2.5
20°	0.7	1	500	4	12	8.1	1.5
10°	0.7	0.2	1000	4	140	55	2.5
10°	0.8	0.2	2000	4	910	200	4.6

Table 1. Times in seconds (given to two significant figures) for the pure Newton method compared to our adapted Broyden–Newton method.
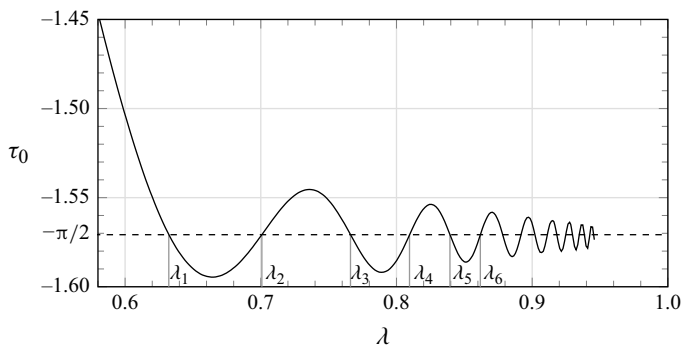
Figure 4. Plot of the angle at the tip of the finger versus λ for $\epsilon^2 = 1$, $\theta_0 = 20°$. Smooth, physical fingers exist at the intersection points where $\tau_0 = -\pi/2$. The asymptotic analysis of the selection mechanism (Andersen *et al.* 2024) shows that there exists a countably infinite number of such selected fingers with associated λ values labelled $\lambda_1(\epsilon) < \lambda_2(\epsilon) < \lambda_3(\epsilon) < \cdots < 1$.

6. Numerical results

The numerical method allows the angle at the tip of the finger (τ_0) to be a free parameter. However, the solutions are physical only if they are smooth, which requires the tip of the finger to have angle $-\pi/2$. In figure 4, we plot the angle at the tip of the finger against λ for $\epsilon^2 = 1$, $\theta_0 = 20°$. We can identify the selected λ values, $\lambda = \lambda_1, \lambda_2, \ldots$, at which $\tau_0 = -\pi/2$.

The physical profiles for the first six selected solutions are shown in figure 5 for $\epsilon^2 = 3$, $\theta_0 = 20°$. The figure shows that small oscillations appear in the profiles near the tips of the fingers. We also see that each successive selected value of $\lambda(\epsilon)$ has an associated physical profile with one additional wavelength of oscillations at the tip. The selection condition can be obtained analytically by analysing these exponentially small contributions to the solution using the techniques from exponential asymptotics. This analysis is done in a separate paper (Andersen *et al.* 2024), and the key ideas were briefly summarised in § 3.

We can measure the amplitude of the oscillations near the tip as ϵ varies. For each value of ϵ, we fix $\lambda = 0.85$ and then use our numerical method to find τ along the free surface. We subtract the leading-order component of τ, associated with zero surface tension, which makes the oscillations easier to identify, as shown in figure 6. The amplitude of the oscillations varies with s, so we measure the amplitudes at a fixed value $s = 0.8$, which lies near the tip of the finger. Since $s = 0.8$ does not necessarily fall at a peak of the oscillations, this requires an approximation of the amplitude, which we obtain by interpolating from the
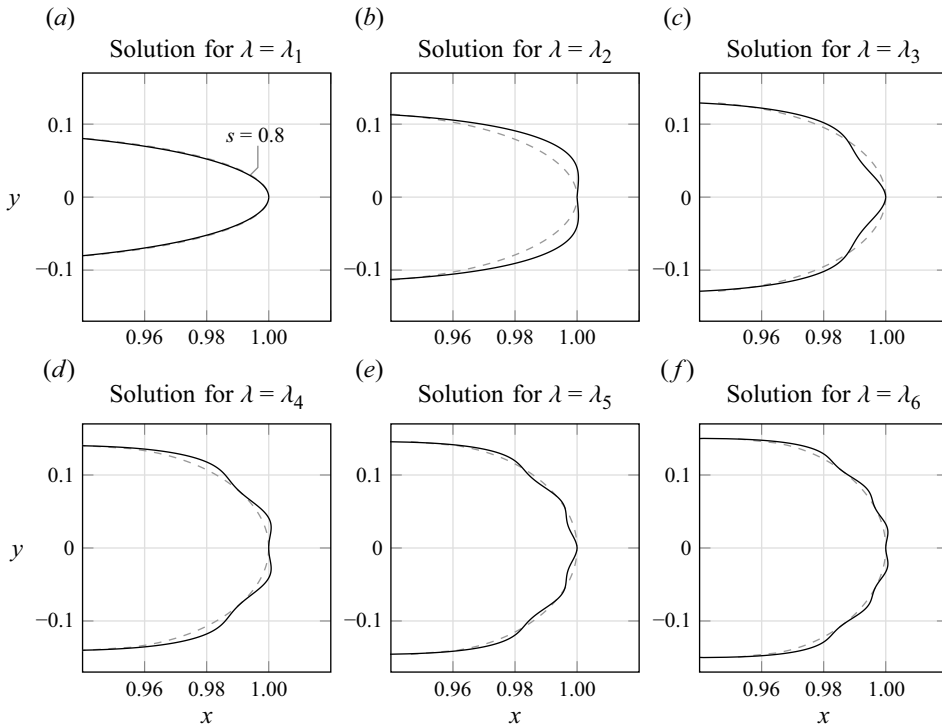
Figure 5. Numerical solutions showing the physical profiles (black) for the first six selected solutions with $\epsilon^2 = 3$, $\theta_0 = 20°$. The interface develops oscillations near the tip of the finger for the higher branches. Here, $\epsilon = 3$ is chosen since this is large enough for the oscillations to be visible. The leading-order solution (x_0, y_0) is shown in grey.
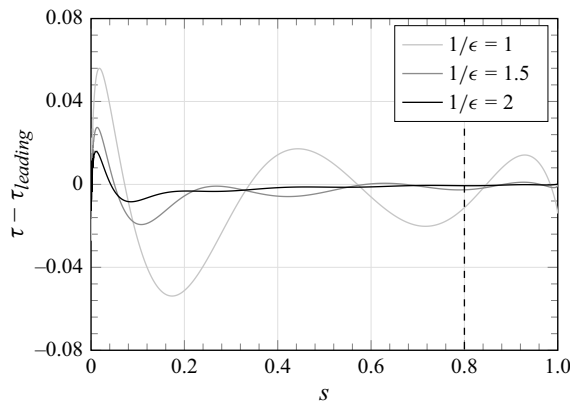

Figure 6. Plot of $\tau - \tau_{leading}$ showing the exponentially small oscillations in the solution. The amplitudes of the oscillations are approximated at $s = 0.8$ by interpolating from neighbouring peaks, and the approximated amplitudes are plotted in figure 7 for different values of ϵ.

amplitudes of the neighbouring peaks. The approximated oscillation amplitude versus $1/\epsilon$ is shown in figure 7.

We see in figure 7 that for a range $1/\epsilon \approx 0.9-1.9$, the logarithm of the oscillation amplitudes follows a straight line with negative gradient (approximate gradient -4.6
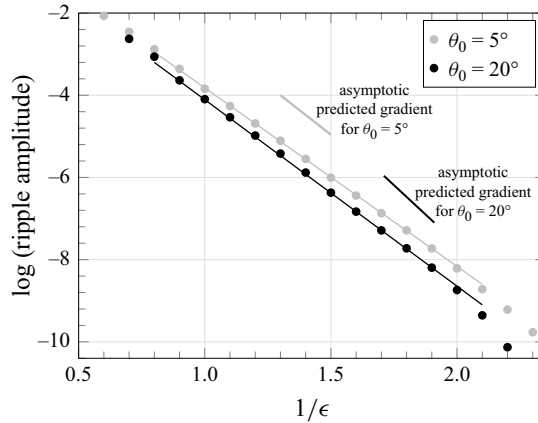
Figure 7. The amplitude of the small oscillations shown in figure 5, measured via τ at $s = 0.8$ as a function of ϵ. These correspond to computations with $N = 1000$, $\lambda = 0.85$ and $\theta_0 = 5°$, $20°$. The straight line shows the line of best fit (approximate gradient -4.6 for $\theta_0 = 20°$, and -4.3 for $\theta_0 = 5°$), confirming exponential smallness in ϵ. The predicted gradient (-5.9 for $\theta_0 = 20°$, and -4.8 for $\theta_0 = 5°$) from the exponential asymptotics for $\theta_0 = 20°$ is also shown.

for $\theta_0 = 20°$, and -4.3 for $\theta_0 = 5°$). This shows that the measured oscillations are exponentially small with respect to the surface tension parameter ϵ, in the limit $\epsilon \to 0$. For $\theta_0 = 20°$, the predicted gradient from the exponential asymptotics is -5.9, and for $\theta_0 = 5°$, the predicted gradient is -4.8.

For larger ϵ values, it is expected that figure 7 will cease to be linear, as the small ϵ approximation breaks down, and nonlinear components will begin to dominate. For smaller ϵ values, the oscillations on the profile become very small and are difficult to identify. To measure the amplitude of these oscillations, we would first need to subtract out the $\mathcal{O}(\epsilon)$ trends; however, the complexity of numerical solutions of higher-order algebraic corrections rivals that of the full nonlinear problem.

Finally, we use the numerical method to find the selected solutions with a smooth tip ($\tau_0 = -\pi/2$), and use numerical continuation to follow the families of selected solutions $\lambda_i(\epsilon)$ for decreasing values of ϵ. Values for these selected families of $\lambda_i(\epsilon)$, $i = 1, 2, \ldots$, are plotted in bifurcation diagrams in figure 8 using $N = 1000$ mesh points. The bifurcation diagrams are compared to exponential asymptotic results from Andersen *et al.* (2024) in figures 8(a)–8(c) for three different wedge angles. We see good agreement between the numerical results and the exponential asymptotics, particularly for higher branches and larger values of ϵ^2.

A numerical error occurs for small ϵ values; however, in figures 8(a)–8(c), we have omitted the numerical results when this error is large. The error is demonstrated in figure 8(d) for the third branch, λ_3, in the case with $\theta_0 = 20°$. Here, the error between the numerical results and exponential asymptotic results increases significantly when $\epsilon^2 < 0.1$. As shown in figure 8(d), with $N = 500, 1000, 2000$, the accuracy can be improved for small ϵ values by increasing the number of mesh points. We have found the error to be $\mathcal{O}(1/N)$ as $N \to \infty$, so a very large number of mesh points would be needed to accurately resolve the bifurcation diagram at low values of ϵ^2.

Further, figures 8(a)–8(c) show that the agreement between the exponential asymptotic results and the numerical results improves for the higher branches. We conjecture that one of the assumptions in the asymptotic theory is violated for the lower branches. The selection condition (3.5) is based on two singularities, ζ_1 and ζ_C, in the complex ζ-plane.
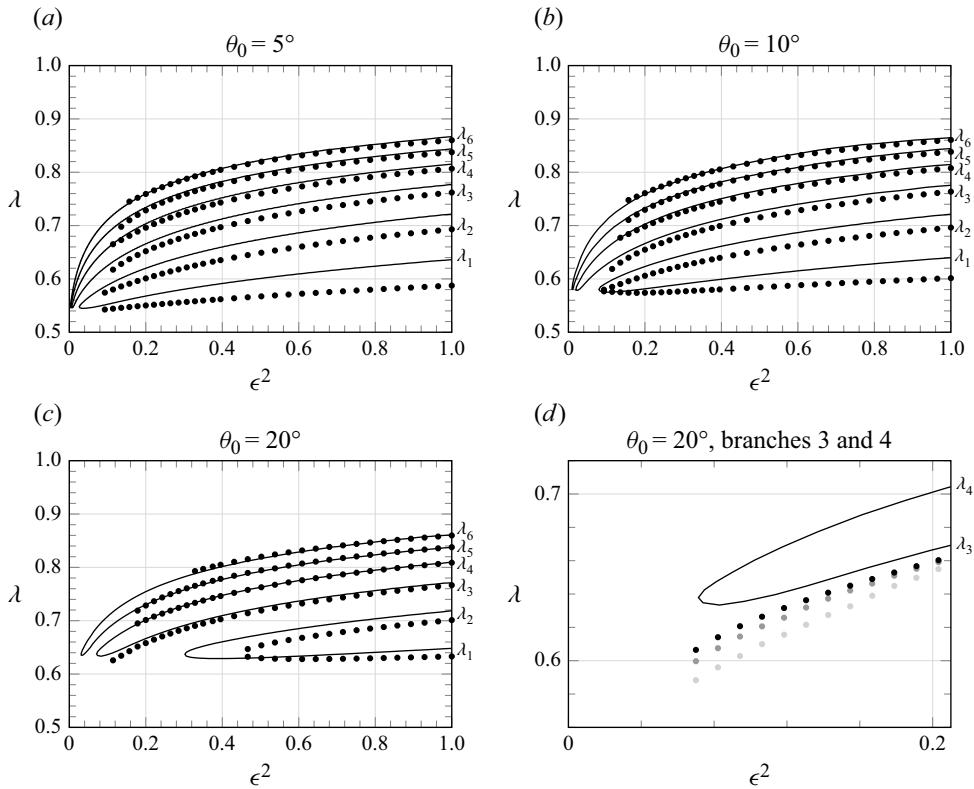
1013 A18-10

Figure 8. Bifurcation diagrams for wedge angles (*a*) $\theta_0 = 5°$, (*b*) $\theta_0 = 10°$ and (*c*) $\theta_0 = 20°$, showing the first six selected λ values for different values of the surface tension parameter ϵ^2. The black curves show the predicted branches found by evaluating (3.5) from the exponential asymptotic analysis in Andersen *et al.* (2024). The dots show the branches predicted using the numerical scheme described in § 5 with $N = 1000$ mesh points. The numerical scheme is able to solve for higher branches than the results of previous numerics for this problem presented in Ben Amar (1991*b*) for $\theta_0 = 20°$. (d) Zoom in on the third and fourth branches from the bifurcation diagram for $\theta_0 = 20°$ with numerical results (dots) for $N = 500$ (light grey), $N = 1000$ (grey), $N = 2000$ (black) mesh points.

In addition, there are branch points at $\zeta = \pm i$. In the dual limit as $\lambda \to 0.5$ and $\theta_0 \to 0$, the singularity ζ_1 approaches the branch point at i. The exponential asymptotic analysis relies on the assumption that the singularities in the complex plane are well separated, and this breaks down in the dual limit. We conjecture that a special regime needs to be considered when the singularity ζ_1 enters the neighbourhood of the branch point at $\zeta = i$, and that this would improve the exponential asymptotic results on the lower branches.

7. Discussion

This paper presents a numerical scheme that solves for the self-similar divergent Saffman–Taylor fingers in a wedge. Using the numerical scheme, we have been able to plot selected solutions and observe the characteristic oscillations on the tips of the fingers. Further, we proved numerically that the oscillation amplitudes are exponentially small in terms of the surface tension parameter ϵ, in the limit $\epsilon \to 0$. Finally, we present the bifurcation diagrams obtained numerically, which are compared to recent exponential asymptotic results. There are a number of interesting extensions to the work in this paper in the fields of Hele-Shaw cells and numerical solutions to free surface problems.

One of the main restrictions to the numerical method used in this paper is the computational cost. The governing equations (2.2), (2.7), (2.8) are evaluated numerically using a number of trapezoidal schemes, which becomes very computationally expensive when a large number of mesh points are used. We find that a large number of mesh points are required ($\mathcal{O}(10^3)$ mesh points) to obtain accurate numerical results for small surface tension values. First, using a larger value of γ distributes more mesh points near the tip of the finger, and means that numerical results of the same accuracy can be obtained with fewer mesh points (for this reason, we use $\gamma = 4$, as is done in Vanden-Broeck 1983). Further, in this work, we implement a novel scheme using a quasi-Newton method (Broyden's method) that greatly increases the speed of the computation. The use of quasi-Newton solvers is well researched in the field of numerical analysis, but to our knowledge, it is rarely applied to this style of problem. Schemes of this style could be used in numerical methods to improve the numerical results of other similar free surface problems that are restricted by their requirement for large numbers of mesh points.

Additionally, in the full circular geometry, a phenomenon known as 'tip-splitting' occurs, where a single finger is observed to split into two narrower fingers. Understanding this behaviour remains an open problem. It is also believed that a tip-splitting instability occurs in the wedge problem after long time when the similarity solution assumption breaks down. Studying a time-dependent model will be necessary to make progress here. We have started work and have written a time-dependent code for the circular geometry based on the numerical method described in Dallaston & McCue (2014). We hope that this will provide an insight into the time-dependent behaviour when the single finger in a wedge approaches a tip-splitting instability, and the progression of the free surface as it divides into two fingers.

Declaration of interests. The authors report no conflict of interest.

REFERENCES

ANDERSEN, C., LUSTRI, C.J., MCCUE, S.W. & TRINH, P.H. 2024 On the selection of Saffman–Taylor viscous fingers for divergent flow in a wedge. *J. Fluid Mech.* **987**, A42.

BEN AMAR, M. 1991*a* Exact self-similar shapes in viscous fingering. *Phys. Rev. A* **43** (10), 5724–5727.

BEN AMAR, M. 1991*b* Viscous fingering in a wedge. *Phys. Rev. A* **44** (6), 3673–3685.

BRENER, E.A., KESSLER, D.A., LEVINE, H. & RAPPEL, W.-J. 1990 Selection of the viscous finger in the 90° geometry. *Europhys. Lett.* **13** (2), 161–166.

BROYDEN, C.G. 1965 A class of methods for solving nonlinear simultaneous equations. *Maths Comput.* **19** (92), 577–593.

CHAPMAN, S.J. 1999 On the rôle of Stokes lines in the selection of Saffman–Taylor fingers with small surface tension. *Eur. J. Appl. Maths* **10** (6), 513–534.

COMBESCOT, R. 1992 Saffman–Taylor fingers in the sector geometry. *Phys. Rev. A* **45** (2), 873–884.

COMBESCOT, R., DOMBRE, T., HAKIM, V., POMEAU, Y. & PUMIR, A. 1986 Shape selection of Saffman–Taylor fingers. *Phys. Rev. Lett.* **56** (19), 2036–2039.

COMBESCOT, R., HAKIM, V., DOMBRE, T., POMEAU, Y. & PUMIR, A. 1988 Analytic theory of the Saffman–Taylor fingers. *Phys. Rev. A* **37** (4), 1270–1283.

DALLASTON, M.C. & MCCUE, S.W. 2014 Corner and finger formation in Hele-Shaw flow with kinetic undercooling regularisation. *Eur. J. Appl. Math.* **25** (6), 707–727.

HONG, D. & LANGER, J. 1986 Analytic theory of the selection mechanism in the Saffman–Taylor problem. *Phys. Rev. Lett.* **56** (19), 2032–2035.

LEVINE, H. & TU, Y. 1992 Mean-field diffusion-limited aggregation in radial geometries. *Phys. Rev. A* **45** (2), 1053–1059.

MCLEAN, J. & SAFFMAN, P. 1981 The effect of surface tension on the shape of fingers in a Hele-Shaw cell. *J. Fluid Mech.* **102**, 455–469.

PATERSON, L. 1981 Radial fingering in a Hele-Shaw cell. *J. Fluid Mech.* **113**, 513–529.

SAFFMAN, P.G. & TAYLOR, G. 1958 The penetration of a fluid into a porous medium or Hele-Shaw cell containing a more viscous liquid. *Proc. R. Soc. Lond. A* **245**, 312–329.

TANVEER, S. 1987 Analytic theory for the selection of a symmetric Saffman–Taylor finger in a Hele-Shaw cell. *Phys. Fluids* **30** (6), 1589–1605.

TANVEER, S. 2000 Surprises in viscous fingering. *J. Fluid Mech.* **409**, 273–308.

THOMÉ, H., RABAUD, M., HAKIM, V. & COUDER, Y. 1989 The Saffman–Taylor instability: from the linear to the circular geometry. *Phys. Fluids A: Fluid Dyn.* **1** (2), 224–240.

TU, Y. 1991 Saffman–Taylor problem in sector geometry: solution and selection. *Phys. Rev. A* **44** (2), 1203–1210.

VANDEN-BROECK, J.-M. 1983 Fingers in a Hele-Shaw cell with surface tension. *Phys. Fluids* **26** (8), 2033–2034.

VANDEN-BROECK, J.-M. 2010 *Gravity-Capillary Free-Surface Flows*. Cambridge University Press.